Contents lists available at ScienceDirect

Chemico-Biological Interactions

Long-term administration of low-dose selenium nanoparticles with different sizes aggravated atherosclerotic lesions and exhibited toxicity in apolipoprotein E-deficient mice

Junying Xiao [a], Hui Cao [a], Siyu Guo [a], Shengze Xiao [a], Na Li [a], Min Li [a], Yuzhou Wu [a,b], Hongmei Liu [a,b,*]

[a] *Hubei Key Laboratory of Bioinorganic Chemistry and Materia Medica, School of Chemistry and Chemical Engineering, Huazhong University of Science and Technology, Wuhan, 430074, China*
[b] *Key Laboratory of Material Chemistry for Energy Conversion and Storage, Ministry of Education, Wuhan, 430074, China*

ARTICLE INFO

ABSTRACT

Exploration of long-term *in vivo* effects of nanomaterials, particularly those with potential biomedical applications, is quite important for better understanding and evaluating their biosafety. Selenium nanoparticles (SeNPs) has been considered as a good candidate in biomedical applications due to its high bioavailability, considerable biological activity, and low toxicity. However, its long-term biological effects and biosafety remain unknown. Our previous study demonstrated that 8-week supplementation with SeNPs (50 μg Se/kg/day) was safe and had an anti-atherosclerotic activity in apolipoprotein E-deficient (ApoE$^{-/-}$) mice, a well-known animal model of atherosclerosis. As a chronic disease, atherosclerosis needs long-term drug therapy. The aim of this study is to investigate the long-term effects of SeNPs with different sizes on atherosclerotic lesions and their biosafety in ApoE$^{-/-}$ mice fed with a high fat diet. Unexpectedly, the results showed that 24-week administration of SeNPs even at a low dose (50 μg Se/kg/day) aggravated atherosclerotic lesions. Furthermore, SeNPs exacerbated oxidative stress by inhibiting the activities of antioxidant enzymes and the expression of antioxidant selenoenzymes. SeNPs also exacerbated hyperlipidaemia by inducing hepatic lipid metabolic disorder. In the meanwhile, SeNPs aggravated organ injury, especially liver and kidney injury. The above adverse effects of SeNPs were size dependent: SeNPs with the size of 40.4 nm showed the highest adverse effects among the SeNPs with three sizes (23.1 nm, 40.4 nm, and 86.8 nm). In conclusion, the present work shows that long-term administration of low-dose SeNPs aggravated atherosclerotic lesions by enhancing oxidative stress and hyperlipidaemia in ApoE$^{-/-}$ mice, indicative of cardiovascular toxicity. Moreover, long-term administration of SeNPs led to injury to liver and kidney. These results offer novel insights for better understanding the biosafety of SeNPs and other biomedical nanomaterials.

1. Introduction

Due to the unique physical and chemical properties, nanomaterials may greatly benefit biological research and medical therapy. Many nanomaterials have exhibited high biodegradability, broad biocompatibility, and low cytotoxicity in cultured cells or *in vivo*, showing great potential in diagnostics, imaging, gene and drug delivery and other types of therapy [1–3]. In the meanwhile, omnipresent nanomaterials

have also aroused a widespread concern of its biosafety. To address such concerns, great efforts have been made to examine short-term effects of nanomaterials on cell survival and proliferation [3–5]. However, compared with the benefit achieved in short-term treatment of nanomaterials, whether these nanomaterials have unexpected effects after long-term exposure is less understood. Many recent works have shown varying degrees of *in vivo* toxicity of nanomaterials over time [6,7]. For instance, gold nanoparticles are generally considered non-toxic to cell

growth in short-term treatment, whereas they might have long-term effects on cellular metabolism and energy homeostasis [6]. However, no matter short- or long-term administration, carbon-based nanoparticles, including diamond, graphene oxide and graphite, had no obvious influence on the health of animals [8]. Therefore, to fully understand the biosafety of nanomaterials, it is quite necessary to explore their long-term effects, particularly for those with promising biomedical applications *in vivo*.

Selenium (Se), as an essential trace element, is of fundamental importance to human health [9,10]. However, the safety window for Se intake is fairly small, excess Se intake is toxic. As a unique form of Se, Se nanoparticles (SeNPs) exhibits higher bioavailability and biological activity, and lower toxicity when compared with the other Se species such as selenious acid, sodium selenite (Na_2SeO_3), selenomethionine (SeMet) and methylselenocysteine (SeMSC) [11–13]. Animal studies have shown that the acute toxicity (at the dose of 10 mg Se/kg/day for 6, 12, 24, and 48 h) and short-term toxicity (at the dose of above 2 mg Se/kg/day for 7–15 days) of SeNPs in mice were less than those of selenite, SeMSC and SeMet [14–16]. Furthermore, 13-week administration of SeNPs at supranutritional levels (0.2–0.4 mg/kg/day) was nontoxic in rats [17]. Recent studies have reported that SeNPs could be served as therapeutic agents in cancer, Alzheimer's disease, diabetes, etc [11–13]. For example, SeNPs were more efficient than selenite in producing reactive oxygen species in cancer cells and thus exhibited better therapeutic activity [18]. SeNPs treatment (100 μg Se/kg/day) for 28 days alleviated hyperglycaemia and hyperlipidaemia in diabetic rats [19]. Therefore, SeNPs, with lower risk for excess supplementation, has been considered as a good candidate to replace other Se species in clinical practice [11–13]. However, the clinical application of SeNPs may require long-term administration, in which the safety margin and potential toxic effects of SeNPs are important considerations. The long-term biological effects and biosafety data of SeNPs are lacking till now.

Atherosclerosis (AS) and related cardiovascular diseases represent the greatest threats to human health worldwide due to high morbidity and mortality [20,21]. AS is a chronic, lipid-driven inflammatory process characterized by the narrowing of the arterial lumen due to the buildup of plaque (mainly made up of fat and cholesterol) inside the arterial wall. Over time, plaque hardens and narrows the arteries, leading to serious cardiovascular diseases, including heart attack, stroke, or even death [20]. Our previous study found that SeNPs at different doses (25, 50, 100 μg Se/kg/day) had anti-atherosclerotic effect in apolipoprotein E-deficient ($ApoE^{-/-}$) mice after oral administration for 8 or 12 weeks [22,23]. Moreover, the medium dose of SeNPs (50 μg Se/kg/day) showed the best effect. However, as a chronic disease, AS needs long-term drug treatment. It is unclear whether long-term administration of SeNPs (LTA-SeNPs) is safe and still has anti-atherosclerotic activity. Besides, within a given geometric shape, a nanomaterial's dimensions are a strong determinant of biological effect. For example, Jiang et al. showed that although all gold and silver nanoparticles within the 2–100 nm size range altered signalling processes essential for basic cell functions (including cell death), 40- and 50-nm nanoparticles demonstrated the greatest effect [24]. Therefore, in the current study, we investigated the effect of LTA-SeNPs (24 weeks, 50 μg Se/kg/day) with different sizes (~20 nm, ~40 nm and ~90 nm) on AS development and their biosafety in high-fat diet fed $ApoE^{-/-}$ mice, a well-known animal model of AS, which may contribute to a better understanding of the biosafety of SeNPs.

2. Materials and methods

2.1. Materials

Na_2SeO_3 was purchased from Sigma-Aldrich. Glutathione (GSH) was purchased from Sinopharm Chemical Reagent Co., Ltd (Shanghai, China). Bovine serum albumin (BSA) was purchased from Biosharp (Hefei, China). The commercial kits for determining triglyceride (TG),

total cholesterol (TC), low-density lipoprotein cholesterol (LDL-C), high-density lipoprotein cholesterol (HDL-C), malonaldehyde (MDA), total superoxide dismutase (SOD) including Cu,Zn-SOD and Mn-SOD, glutathione peroxidases (GPx), alanine aminotransferase (ALT), aspartate aminotransferase (AST), creatine kinase (CK) and blood urea nitrogen (BUN) were purchased from Nanjing Jiancheng Institute of Biological Engineering (Nanjing, China). Trizol, First Strand cDNA Synthesis kit, SYBR Green PCR Master Mix kit were purchased from Thermo Fisher Scientific. All chemicals were of analytical grade and used without further purification.

2.2. Preparation of SeNPs with different sizes

SeNPs with average size of 40.4 nm (named as SeNPs-2) were prepared by reducing Na_2SeO_3 with GSH in the presence of BSA as a stabilizer according to our previous work with little modification [23,25]. Briefly, Na_2SeO_3 was mixed with BSA under vigorous stirring, and GSH was dropwise added into the mixture. The final volume of the mixture was 10 mL and the final concentrations of Na_2SeO_3, GSH and BSA were 2 mM, 8 mM and 1 mg/mL, respectively. The colour of the mixture turned into red upon adding 25 μL NaOH (2 M), which indicated that SeNPs were formed. Thereafter, the reaction system was stirred for another 30 min and centrifuged immediately with 12000 rpm at 4 °C for 20 min to stop the reaction. The resulting red precipitate was washed three times by centrifugation with double distilled water. Finally, as-prepared SeNPs were suspended in double distilled water and stored at 4 °C for further use. Based on the above procedure, SeNPs with average size of 23.1 nm (named as SeNPs-1) and 86.8 nm (named as SeNPs-3) were obtained by varying the concentrations of Na_2SeO_3, GSH and BSA, reaction time and centrifugation rate. The reaction conditions for the synthesis of SeNPs with three different sizes were listed in Table S1.

2.3. Characterization of SeNPs with different sizes

The hydrodynamic size of the as-prepared SeNPs was measured by dynamic light scattering (DLS) (LB-550, Horiba, Ltd. Japan). The morphology of those SeNPs was observed by transmission electron microscope (TEM) (HT7700, HITACHI Co., Japan). Infrared (IR) spectra of the samples were recorded on IR spectrometer (Equinox 55, Brucker Optics, Germany) in the range of 4000-500 cm^{-1} using the KBr-disk method. X-ray diffraction (XRD) (SmartLab-SESmartLab-SE, Nippon Neoku Co., Ltd, Japan) patterns of the samples were detected with the 2θ range 10°–80°. X-ray photoelectron spectra (XPS) spectra were obtained using a photoelectron spectrometer (AXIS-ULTRA DLD-600W, Shimadzu-Kratos, Japan).

2.4. Animals and experimental design

$ApoE^{-/-}$ mice, the most used animal model of AS [26], were used in this study. Seven-week-old male $ApoE^{-/-}$ mice (C57BL/6 background) were purchased from Beijing Vital River Laboratory Animal Technology Co., Ltd. After adaptive feeding with a standard diet for 1 week, all $ApoE^{-/-}$ mice were fed with a high-fat diet (HFD, containing 21% cream and 0.15% cholesterol, obtained from Jiangsu Medicience Biomedicine Co. Ltd, China) and randomly divided into 5 groups (n = 8 in each group): AS model group (Model), Na_2SeO_3 group, the different sizes of SeNPs groups, containing SeNPs-1 group, SeNPs-2 group, and SeNPs-3 group. The Na_2SeO_3 group and SeNPs groups were treated with Na_2SeO_3 and different sizes of SeNPs (50 μg Se/kg body weight) per day via an intragastric administration, respectively. The Model group was kept without any treatment except intragastric administration of normal saline per day. Sex- and age-matched C57BL/6 mice (n = 8) from Hubei Provincial Center for Disease Control and Prevention were fed with standard diet and used as reference control (WT group). All animals were housed in plastic cages (4 mice per cage) with free access to water
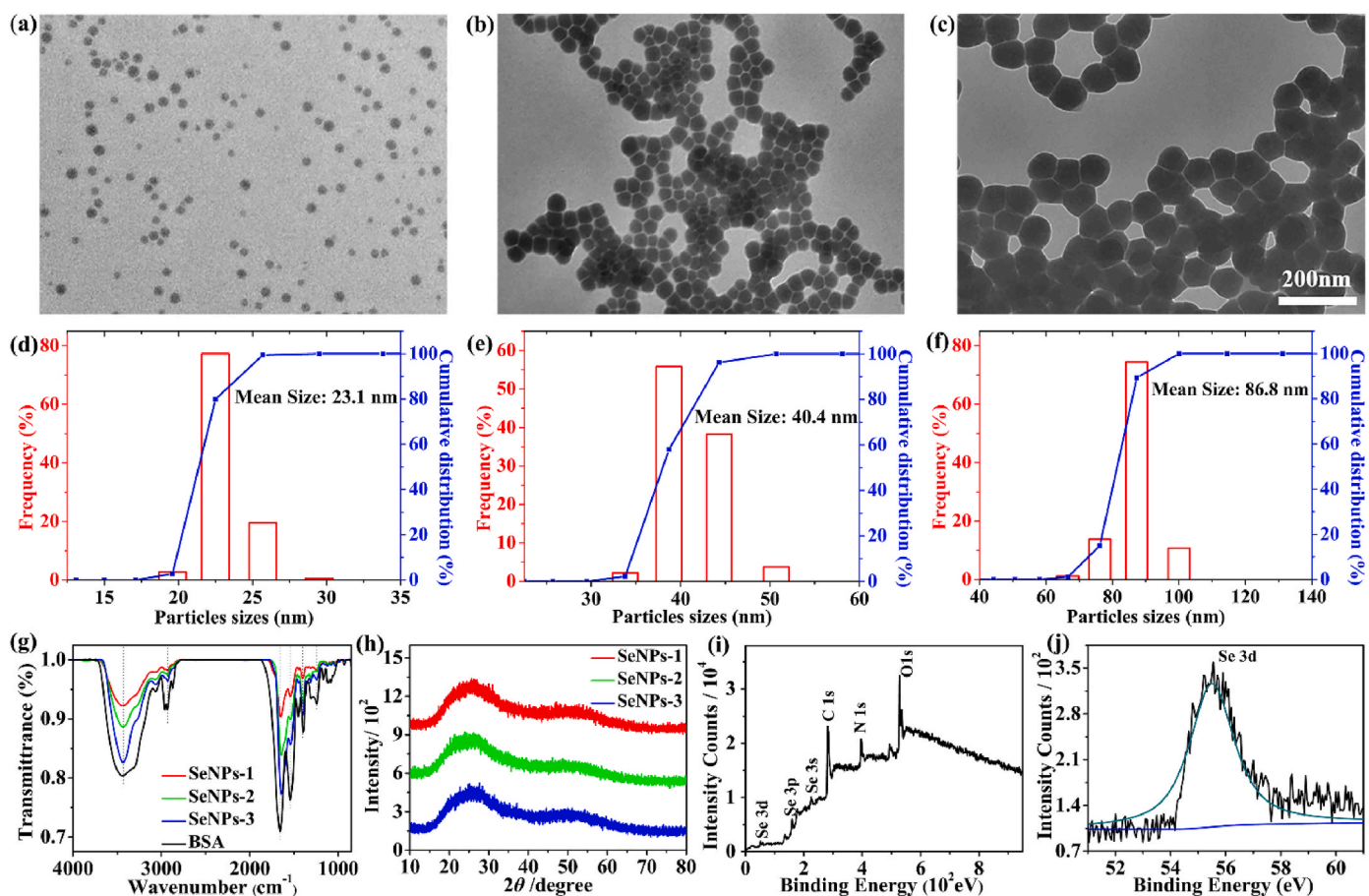
Fig. 1. Characterization of the SeNPs with three different sizes. (a) TEM of SeNPs-1. (b) TEM of SeNPs-2. (c) TEM of SeNPs-3. (d) DLS of SeNPs-1. (e) DLS of SeNPs-2. (f) DLS of SeNPs-3. (g) IR spectra. (h) XRD curve. (i) and (j) XPS curve of SeNPs-2.

and food and the feeding environment was in controlling (22 ± 2 °C, 12 h light/dark cycle). Body weights of the mice were recorded weekly throughout the experimental period. After 24 weeks feeding, all mice were fasted overnight and euthanized by intraperitoneal injection of pentobarbital sodium. Blood and tissue samples were then obtained quickly for further analysis. The schematic design of animal experiments was showed in Scheme S1. All animal experiments were approved by the local Ethics Committee of Huazhong University of Science and Technology (No. s1900).

2.5. Sampling

At the end of the experiment, blood samples were obtained through transthoracic cardiocentesis. The serum was separated from blood by centrifugation at 3500 rpm for 15 min at 4 °C and kept in aliquots at −80 °C until the determination of biochemical indices. Immediately after blood drainage, all mice were perfused with 0.01 M phosphate buffer saline (PBS) via the left ventricle until no residual blood was apparent in the perfusate. The whole aorta was immediately removed and fixed in 4% paraformaldehyde solution. The liver, kidney, heart and lung were collected. Some portions of these tissues were fixed in 4% paraformaldehyde for histopathological analysis, while other portions were preserved at −80 °C for other studies.

2.6. Atherosclerotic lesion analysis

To determine the severity of atherosclerotic lesion, the whole aorta (from the aortic root to the iliac bifurcation) was opened longitudinally and *en face* Oil Red O staining was performed as previously described [27,28]. The percentage of the Oil Red O-positive area compared with whole aorta surface area was quantified using Image Pro Plus 6.0 software and used as the relative atherosclerotic plaque area in the entire aorta. For atherosclerotic lesion analysis in aortic root, paraffin sections of aortic root were stained with hematoxylin-eosin (HE) and microscopic examination was performed. The percentage of the plaque area compared with the area of aortic root section was quantified using Image Pro Plus 6.0 software and used as the relative atherosclerotic plaque area in aortic root.

2.7. Biochemical analysis

The levels of serum TG, TC, HDL-C, LDL-C, MDA, and BUN, and the activities of SOD, GPx, ALT, AST, and CK were tested according to the manufacturer's instructions of the commercial kits. A microplate analyzer (Infinite M200 PRO NanoQuant, TECAN, Switzerland) was used to determine the absorbance of the samples at the corresponding wavelength. An internal quality control was employed to keep the measurement process reliable in the determination of all biochemical indices. MDA level was calculated by detecting the optical density (OD)
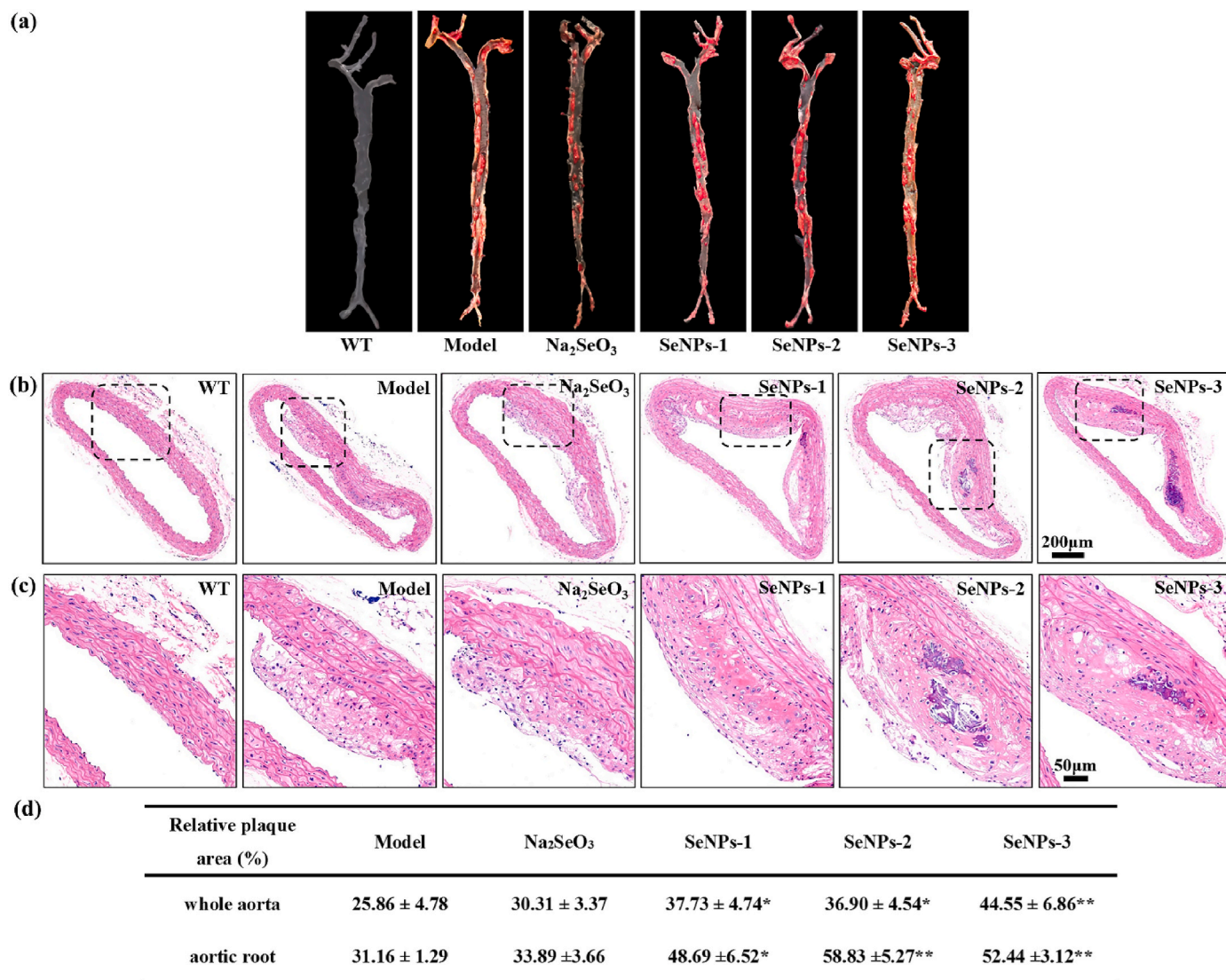
Fig. 2. Effect of LTA-SeNPs on atherosclerotic lesions formation in aorta. (a) Representative images of Oil Red O-stained whole aorta. (b) Representative images of HE-stained cross-section of aortic root (50 ×). (c) Magnified views corresponding to the black rectangles in (b) (150 ×). (d) Quantitative percentage of relative plaque area (Oil Red O-positive area) in whole aorta compared with whole aorta surface area and in aortic root compared with the area of aortic root section. The results were expressed as mean ± SD (n = 5). *P < 0.05, **P < 0.01, compared with the AS Model group. (For interpretation of the references to colour in this figure legend, the reader is referred to the Web version of this article.)

of sample, control of sample, blank and standard substance at 532 nm according to the following equation:

$$\text{Serum MDA level(nmol / mL)} = \frac{OD(Sample) \; - \; OD(Control)}{OD(Standard) \; - \; OD(Blank)} \; \times \; c(Standard)$$

2.8. Histopathological analysis

Paraffin sections of liver, kidney, heart and lung of six mice from each group were stained with HE for histopathological analysis according routine histological procedures. Additionally, Oil Red O staining of liver section of six mice from each group was performed in order to observe the lipid deposition. At least three different fields of each Oil Red O staining section of liver were captured for the quantitative statistics. The percentage of the Oil Red O-positive area compared with total section area of liver was quantified using Image Pro Plus 6.0 software.

2.9. Determination of gene expression by quantitative real-time polymerase chain reaction (RT-PCR)

The mRNA expression levels of low density lipoprotein receptor (LDLR), hydroxymethyl glutarate mononyl CoA reductase (HMGCR), cholesterol 7 alpha-hydroxylase (CYP7A1), ATP-binding cassette transporters subfamily G members (ABCG5), fatty acid synthase (FAS), GPx1, and thioredoxin reductases (TrxR1 and TrxR2) in liver of ApoE$^{-/-}$ mice were measured by RT-PCR. Briefly, total RNA was isolated from homogenizing liver tissues using Trizol reagent and reverse-transcribed into cDNA. PCR amplification was performed on an ABI StepOne™ Real-Time PCR System (Applied Biosystems, USA) using the SYBR Green PCR Master Mix kit. Both reverse transcription and PCR amplification were done according to the vendor's protocol. All primers sequences used in this study were listed in Table S2. Quantification was performed using the $2^{-\Delta\Delta CT}$ method by StepOne Plus Software v2.3 with β-actin gene as internal control [29].

Table 1
Effect of LTA-SeNPs on serum MDA level, and the activities of SOD and GPx.

	MDA (nmol/mL)	SOD (U/mL)	GPx (U/mL)
WT	0.78 ± 0.11	84.59 ± 8.19	364.53 ± 44.28
Model	$18.15 \pm 0.69^{###}$	77.39 ± 4.16	329.35 ± 36.54
Na_2SeO_3	16.67 ± 2.85	$97.81 \pm 8.88^{**}$	$211.84 \pm 42.23^{*}$
SeNPs-1	18.13 ± 2.22	74.41 ± 6.07	$263.84 \pm 14.00^{*}$
SeNPs-2	18.75 ± 2.21	$64.48 \pm 5.96^{**}$	$260.18 \pm 19.42^{*}$
SeNPs-3	18.75 ± 1.05	$53.04 \pm 6.39^{**}$	$234.29 \pm 42.31^{*}$

Note: The results were expressed as mean $\pm$ SD (n = 6–8). $^{###}P < 0.001$, compared with the WT group. $^{*}P < 0.05$, $^{**}P < 0.01$, compared with the AS Model group.

2.10. Statistical analysis

The results from a representative of at least three independent experiments were expressed as mean $\pm$ SD. One-way ANOVA analysis was employed to analyze differences among groups. Tamhane's T2 test was used to compare the differences between groups when the variance was not uniform. A difference with P < 0.05 was considered significant. Statistical analyses were performed using SPSS 22.0 software.

3. Results

3.1. Characterization of SeNPs

TEM images showed that three types of SeNPs were uniformly spherical in shape, but their sizes were notably difference (Fig. 1a–c). DLS results showed that the mean sizes were 23.1 nm for SeNPs-1, 40.4 nm for SeNPs-2 and 86.8 nm for SeNPs-3, respectively (Fig. 1d–f), which was conformed to the expectation of the experiment.

IR spectra of the SeNPs with different sizes were similar and consistent with that of pure BSA (Fig. 1g), indicating the presence of BSA in SeNPs. Similar XRD pattern of different sizes of SeNPs were obtained. There was no sharp Bragg reflection peak and only two broad peaks at the 2θ angle around 26° and 52° (Fig. 1h), which indicated the as-synthesized SeNPs was amorphous [25]. Taking SeNPs-2 as an example, the elements of Se, C, N and O of SeNPs were observed in XPS pattern (Fig. 1i), which conformed to the element characteristics of SeNPs decorated with BSA. In addition, a distinct peak for Se 3d was at about 55.3 eV (Fig. 1j), which confirmed that the as-synthesized SeNPs was composed of element Se (0) [25].

3.2. LTA-SeNPs aggravated the formation of atherosclerotic lesions in ApoE$^{-/-}$ mice

Oil Red O staining of entire aorta showed that atherosclerotic lesion area was increased by 46.1%, 43.0%, and 72.5% respectively, in SeNPs-1, SeNPs-2 and SeNPs-3 treated groups, compared with the AS Model group (Fig. 2 a, d). It was really unexpected since our previous work showed that 8-week supplement of SeNPs with an average size of 37.2

Table 2
Effect of LTA-SeNPs on blood lipids of ApoE$^{-/-}$ mice.

	TC (mmol/L)	TG (mmol/L)	LDL-C (mmol/L)	HDL-C (mmol/L)
WT	2.69 ± 0.30	0.33 ± 0.06	0.22 ± 0.06	2.46 ± 0.26
Model	$29.18 \pm 4.89^{###}$	$3.23 \pm 0.66^{###}$	$7.58 \pm 1.46^{###}$	$1.41 \pm 0.13^{###}$
Na_2SeO_3	31.72 ± 3.05	$5.04 \pm 0.45^{**}$	$11.46 \pm 2.01^{**}$	$2.61 \pm 0.23^{***}$
SeNPs-1	31.77 ± 2.22	4.03 ± 0.68	$10.54 \pm 1.28^{*}$	$3.09 \pm 0.72^{**}$
SeNPs-2	33.93 ± 6.30	$5.51 \pm 0.71^{***}$	$10.65 \pm 1.75^{*}$	$5.03 \pm 0.37^{***###}$
SeNPs-3	$38.30 \pm 5.96^{*}$	$4.72 \pm 0.57^{**}$	$10.76 \pm 1.44^{**}$	$4.10 \pm 0.68^{***###}$

Note: The results were expressed as mean $\pm$ SD (n = 6–8). $^{###}P < 0.001$, compared with the WT group. $^{*}P < 0.05$, $^{**}P < 0.01$, $^{***}P < 0.001$, compared with the AS Model group.

nm appeared to have a potential for prevention of AS by alleviating hyperlipidaemia and vascular injury in ApoE$^{-/-}$ mice [23]. No significant difference of plaque area was found in Na_2SeO_3 treated group compared to AS Model group, though an increased trend was observed.

HE staining of aortic root was performed to further confirm the effect of LTA-SeNPs on atherosclerotic lesions formation. In the AS Model group, the vessel wall of aortic root was significantly thickened (Fig. 2b), and there were atherosclerotic plaques rich in foam cells, lipids, and proliferated and randomly arranged vascular smooth muscle cells (Fig. 2c). These lesions were further aggravated in LTA-SeNPs treated group (Fig. 2b and c). The relative plaque area based on HE staining was increased from $31.2 \pm 1.3\%$ (AS Model group) to $48.7 \pm 6.5\%$, $58.8 \pm 5.3\%$ and $52.4 \pm 3.1\%$ in SeNPs-1 group, SeNPs-2 group and SeNPs-3 group, respectively (Fig. 2d). As a comparison, there was no significant difference in plaque area between AS Model group and Na_2SeO_3 treated group.

Taken together, the above results indicated that 24-week administration of SeNPs even at a low dose (50 μg Se/kg/day) aggravated atherosclerotic lesions while Na_2SeO_3 had no obvious effect in ApoE$^{-/-}$ mice fed HFD. The aggravated effect of SeNPs-1 with smaller size (23.1 nm) was relatively smaller while those of SeNPs-2 and SeNPs-3 with larger size (40.4 nm and 86.8 nm) were relatively higher.

3.3. Effect of LTA-SeNPs on oxidative stress in the serum of ApoE$^{-/-}$ mice

Compared with the WT group, the level of serum MDA, an end product of lipid peroxidation, was significantly increased in the AS Model group (Table 1), indicating the injury of oxidative stress occurred. Compared with the AS Model group, there was no significant change of serum MDA level in all the SeNPs treated groups. However, the activities of serum SOD and GPx were significantly inhibited by LTA-SeNPs treatment. And the inhibitory effects were gradually aggravated as the size of SeNPs increased (Table 1).
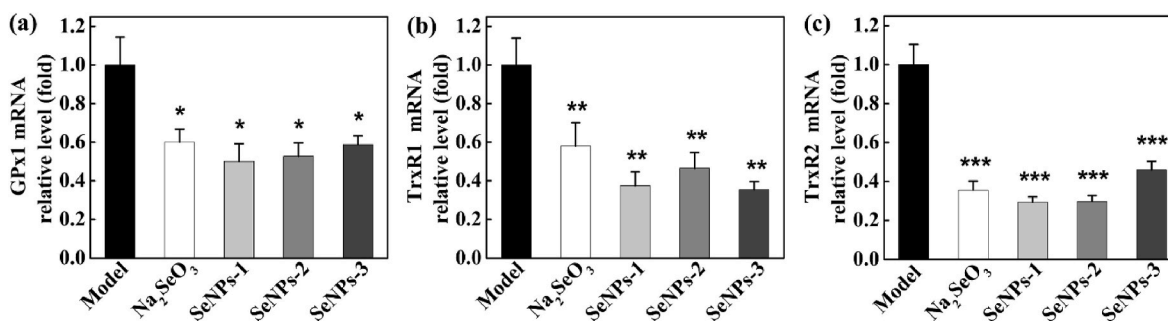

Fig. 3. Effect of LTA-SeNPs on mRNA levels of selenoenzymes in the liver of ApoE$^{-/-}$ mice. Data are normalized with β-actin and the results are expressed as mean $\pm$ SD (n = 4–5). $^{*}P < 0.05$, $^{**}P < 0.01$, $^{***}P < 0.001$, compared with the AS Model group.
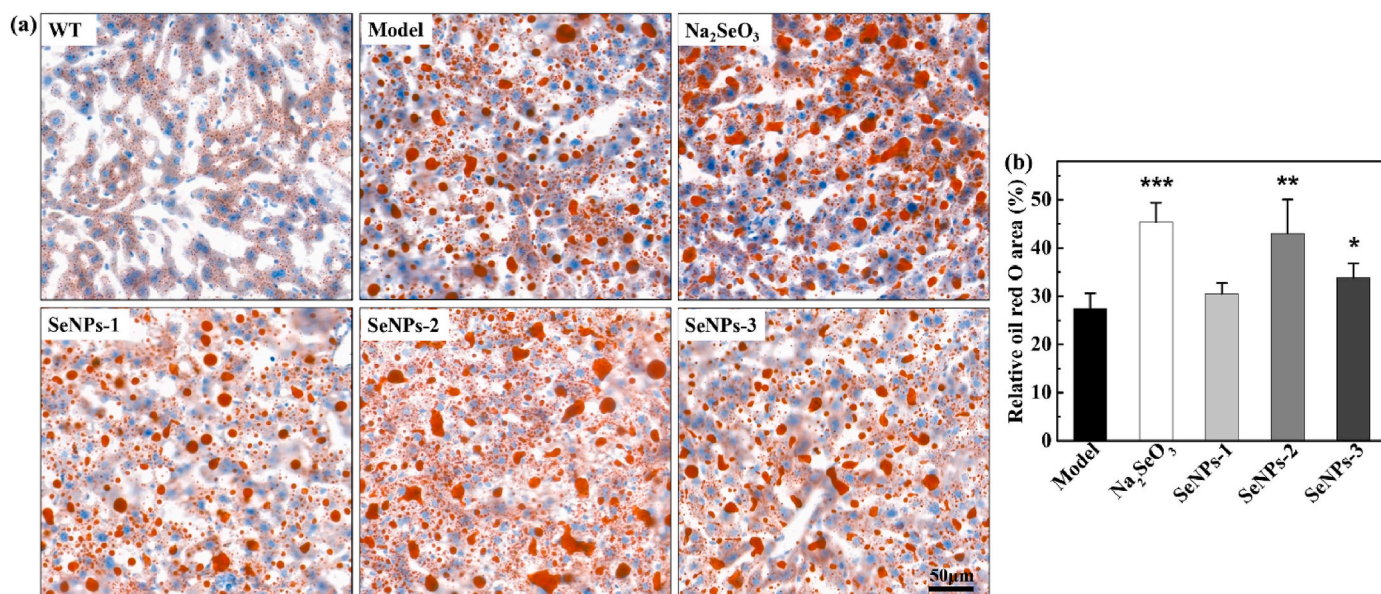
Fig. 4. Effect of LTA-SeNPs on the lipid deposition in liver. (a) Representative images of Oil Red O-stained section of liver (200 ×). (b) Quantitative percentage of Oil Red O staining area compared with total section area. At least three different fields in each section were used for the quantitative statistics. The results were expressed as mean ± SD (n = 6–8). *P < 0.05, **P < 0.01, ***P < 0.001, compared with the AS Model group. (For interpretation of the references to colour in this figure legend, the reader is referred to the Web version of this article.)

Compared with the AS Model group, serum GPx activity in the Na$_2$SeO$_3$ treated group was decreased 35.7% and even lower than that of the SeNPs treated groups. However, serum SOD activity in the Na$_2$SeO$_3$ treated group was increased 26.4% (Table 1), which might partially remedy the adverse effect of decreased GPx activity.

3.4. LTA-SeNPs inhibited the expression of selenoenzymes in the liver of ApoE$^{-/-}$ mice

The expression of three selenoenzymes, GPx1, TrxR1 and TrxR2, in the liver of ApoE$^{-/-}$ mice were detected by RT-PCR. Unexpectedly, their expression levels in LTA-SeNPs treated groups were all markedly

decreased when compared with the AS Model group. The similar trend was observed in Na$_2$SeO$_3$ treated group (Fig. 3). The decreased expression of three selenoenzymes in the liver of ApoE$^{-/-}$ mice might be due to liver injury induced by LTA-SeNPs and Na$_2$SeO$_3$ as demonstrated below.

3.5. LTA-SeNPs aggravated hyperlipidaemia in ApoE$^{-/-}$ mice

Compared with the WT group, the levels of serum TG, TC and LDL-C in AS Model group were significantly increased, while the serum HDL-C level was significantly decreased, which indicated that hyperlipidaemia was successfully induced by HFD in ApoE$^{-/-}$ mice (Table 2). Regrettably, hyperlipidaemia was further exacerbated by LTA-SeNPs. Compared to
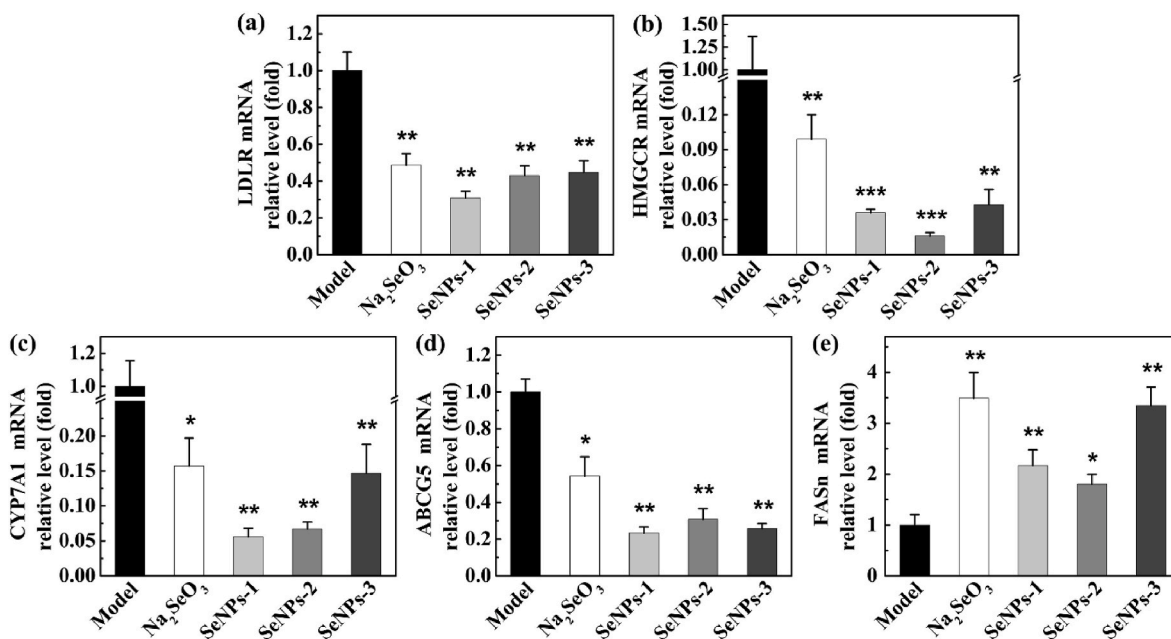

Fig. 5. Effect of LTA-SeNPs on mRNA levels of key genes associated with lipid metabolism. Data are normalized with β-actin and the results were expressed as mean ± SD (n = 4–5). *P < 0.05, **P < 0.01, ***P < 0.001, compared with the AS Model group.

the AS Model group, serum LDL-C level in the SeNPs-1 treated group was increased by 39.1%; the levels of serum TG and LDL-C in the SeNPs-2 treated group were increased by 70.6% and 40.5%, respectively; the levels of serum TC, TG and LDL-C in the SeNPs-3 treated group were increased by 31.3%, 46.1% and 42.0%, respectively. Similarly, the levels of serum TG and LDL-C in the Na_2SeO_3 treated group were increased by 56.1% and 51.2%, respectively (Table 2). Furthermore, the level of serum HDL-C in all the SeNPs treated groups was extremely high, and even higher than that in WT group (Table 2). Taken together, our data revealed that LTA-SeNPs aggravated hyperlipidaemia in HFD fed ApoE$^{-/-}$ mice. In addition, as the size of SeNPs increased, so did the aggravation trend.

3.6. LTA-SeNPs aggravated lipid deposition by inducing lipid metabolic disorder in the liver of ApoE$^{-/-}$ mice

The liver is the central metabolic organ that regulates several key aspects of lipid metabolism [30]. The aggravated hyperlipidaemia in LTA-SeNPs treated ApoE$^{-/-}$ mice might be due to the lipid metabolic disorder in liver. Therefore, we next analysed the lipid deposition by Oil Red O staining and the expression of key genes associated with lipid metabolism by RT-PCR in the liver of ApoE$^{-/-}$ mice.

As shown in Fig. 4a, a large Oil Red O-positive area in the section of liver was observed in the AS Model group, the LTA-SeNPs treated groups and the Na_2SeO_3 treated group, indicating that the lipid deposition induced by HFD occurred in the liver. Quantification based on Oil Red O-staining of hepatic section showed that the relative lipid deposition area was significantly increased from $27.46 \pm 3.13\%$ (AS Model group) to $43.04 \pm 6.98\%$ and $33.79 \pm 2.97\%$ in the group of SeNPs-2 and SeNPs-3, respectively. No significant increase of the relative lipid deposition area was observed in the SeNPs-1 treated groups. The relative lipid deposition area of the Na_2SeO_3 treated group was markedly increased compared with the AS Model group, and was even higher than that of all the SeNPs treated groups (Fig. 4b).

Fig. 5 showed the mRNA expression levels of key genes associated with lipid metabolism in the liver of ApoE$^{-/-}$ mice. LDLR was responsible for LDL-C uptake by hepatocytes [31]. The decreased expression of LDLR means the decreased uptake of serum LDL-C by hepatocyte, thus leading to increased serum LDL-C. Compared with the AS Model group, the mRNA expression level of hepatic LDLR was dramatically inhibited in all the SeNPs treated groups (Fig. 5a), which provided an explanation for the increase of serum LDL-C observed in LTA-SeNPs treated groups. HMGCR, a classical rate-limiting enzyme for cholesterol biosynthesis, catalyzed the conversion of HMG-CoA to mevalonic acid, a necessary step in cholesterol biosynthesis [32]. CYP7A1 and ABCG5, two key enzymes involved in the decomposition and excretion of cholesterol, have opposite effect on cholesterol biosynthesis compared with HMGCR [33, 34]. LTA-SeNPs treatment not only significantly inhibited the expression of HMGCR (Fig. 5b), but also the expression of CYP7A1 and ABCG5 compared with the AS Model group (Fig. 5c and d). We speculated that the inhibitory effect of LTA-SeNPs on the expression of CYP7A1 and ABCG5 exceeded their inhibitory effect on HMGCR, thus resulting in the increased lipid deposition in the liver of the animals in the LTA-SeNPs treated groups as observed in Fig. 4. FAS was a pivotal multi-enzyme protein that catalyzes fatty acid synthesis [31]. Compared with the AS Model group, the expression of FAS was increased significantly in the LTA-SeNPs treated groups (Fig. 5e), which might contribute to the accumulation of lipid in the liver and the aggravation of hyperlipidaemia. In the Na_2SeO_3 treated group, the expression levels of these genes involved in lipid metabolism exhibited the similar trend to the LTA-SeNPs group (Fig. 5). This means that long-term administration of Se, in the form of either SeNPs or Na_2SeO_3, could lead to lipid metabolic disorder in liver.

Table 3
Effect of LTA-SeNPs on the levels of serum biochemistry indices.

	ALT (U/L)	AST (U/L)	CK (U/mL)	BUN (mmol/L)
WT	8.99 ± 1.73	10.90 ± 1.47	0.182 ± 0.015	9.17 ± 0.87
Model	$14.21 \pm 1.69^{\#\#}$	$18.49 \pm 2.15^{\#\#}$	$0.352 \pm 0.068^{\#\#\#}$	$15.08 \pm 2.67^{\#\#}$
Na_2SeO_3	$20.27 \pm 2.32^*$	$27.41 \pm 3.32^{**}$	$0.594 \pm 0.081^{**}$	$19.69 \pm 2.14^*$
SeNPs-1	$19.02 \pm 2.73^*$	20.03 ± 2.57	0.320 ± 0.045	$22.56 \pm 1.84^{**}$
SeNPs-2	$21.73 \pm 2.46^{**}$	22.12 ± 2.89	0.318 ± 0.064	$23.91 \pm 1.80^{**}$
SeNPs-3	$17.92 \pm 2.68^*$	19.73 ± 2.62	0.323 ± 0.037	15.99 ± 2.02

Note: The results were expressed as mean $\pm$ SD (n = 6–8). $^{\#\#}P < 0.01$, $^{\#\#\#}P < 0.001$, compared with the WT group. $^*P < 0.05$, $^{**}P < 0.01$, $^{***}P < 0.001$, compared with the AS Model group.

3.7. Effect of LTA-SeNPs on the body weight and the serum biochemistry indices in ApoE$^{-/-}$ mice

As stated above, LTA-SeNPs with different sizes even at a low dose aggravated atherosclerotic lesions, oxidative stress and hyperlipidaemia. These adverse effects of LTA-SeNPs implied that they might be toxic to the body. Next, of the body weight and serum biochemistry indices were examined to assess the toxicity of LTA-SeNPs.

Compared with the AS Model group, no significant difference was observed in the body weight of LTA-SeNPs treated groups during the experimental period (Fig. S1), suggesting that oral administration of SeNPs for 24 weeks had no significant effect on the overall growth of ApoE$^{-/-}$ mice. However, the change of some serum biochemistry indices implied the organ injury occurred in SeNPs treated mice (Table 3). The increasing activities of serum ALT, AST, CK, and BUN level sensitively reflect the injury of liver (ALT and AST), heart (AST and CK) and kidney (BUN), respectively. All these serum biochemistry indices in AS Model group were significantly increased (P < 0.01) compared with the WT group, indicating the injury of liver, kidney and heart occurred after feeding with HFD for a long term (Table 3). Compared with the AS Model group, serum ALT activity was increased significantly in all the SeNPs treated groups and serum BUN level was increased significantly in the SeNPs-1 and SeNPs-2 treated groups. The highest ALT activity and BUN level were observed in the SeNPs-2 treated group. These data suggested that LTA-SeNPs, especially SeNPs-2, exacerbated the injury of liver and kidney in HFD fed ApoE$^{-/-}$ mice and exhibited a certain extent of toxicity. No significant difference in serum AST and CK activities in all LTA-SeNPs treated groups were observed compared to the AS Model group, indicating that LTA-SeNPs did not affect the heart. Unfortunately, the levels of all serum biochemistry indices were significantly higher in the Na_2SeO_3 treated group than those in the AS Model group.

3.8. Effect of LTA-SeNPs on histopathological changes of main organs in ApoE$^{-/-}$ mice

For further verification of the toxicity of LTA-SeNPs, the histopathological features of liver, kidney, heart and lung were observed by HE staining (Fig. 6).

HE staining of the liver from the AS Model group showed the evidence of fuzzy cellular structure, cellular edema, inflammatory cell infiltration (red arrow) and a large number of lipid droplet (red circle). Besides, extensive unordered hepatocytes resulted in the destruction of hepatic lobule structure in the AS Model group. Disappointedly, these histopathological alterations were aggravated in all the LTA-SeNPs treated groups, especially in SeNPs-2 group. Similarly, Na_2SeO_3 treatment also significantly enhanced histopathological alterations. Taken together, LTA-SeNPs exhibited toxicity to the liver and the toxicity of SeNPs-2 and Na_2SeO_3 were more serious, which was consistent with the above results of serum ALT.
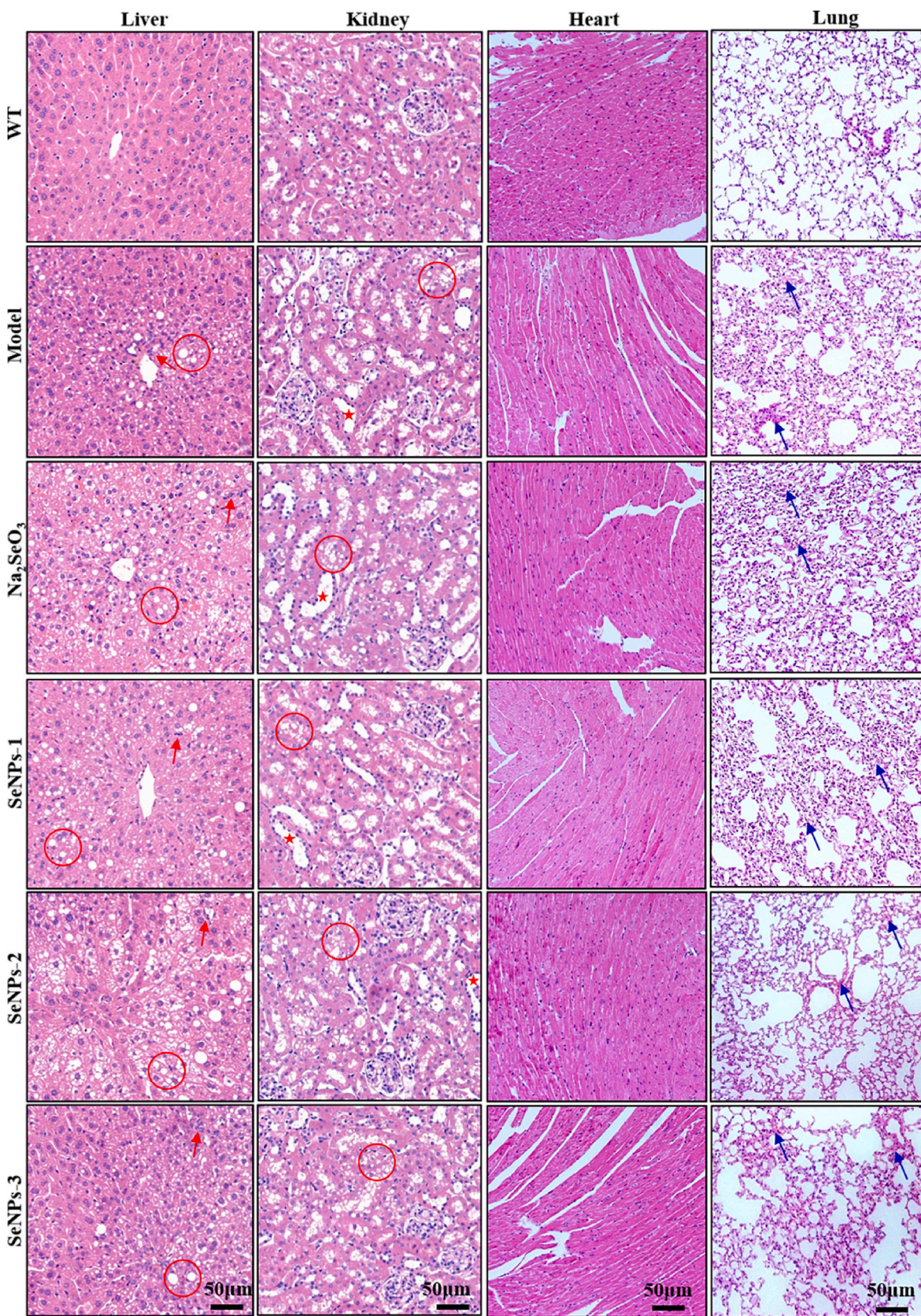
Fig. 6. Effect of LTA-SeNPs on the histopathological alteration of the liver, kidney, heart and lung in ApoE$^{-/-}$ mice. Representative images of HE-stained section of liver, kidney, heart and lung were presented (200 ×). Red arrows refer to inflammatory cell infiltration in liver. Red circles refer to lipid droplet in liver and kidney. Red stars refer to tubular cytoplasmic vacuolation in kidney. Blue arrows refer to neutrophil inflammation in lung. (For interpretation of the references to colour in this figure legend, the reader is referred to the Web version of this article.)

HE staining of the kidney from AS Model group showed a large number of tubular cytoplasmic vacuolation (red star) and lipid droplet (red circle), indicating the kidney injury occurred. Long-term treatment with SeNPs or Na$_2$SeO$_3$ exacerbated these histopathological alterations, especial in the Na$_2$SeO$_3$, SeNPs-1 and SeNPs-2 groups. This was consistent with the above results of serum BUN and further confirmed the toxicity of LTA-SeNPs and Na$_2$SeO$_3$ to the kidney. Moreover, our results demonstrated that the long-term toxicity of SeNPs with smaller size (23.1 and 40.4 nm) to the kidney was much higher than that of SeNPs with larger size (86.8 nm).

HE staining of the heart showed no histopathological change among all the groups. HE staining of the lung from the AS Model group showed a large amount of pulmonary neutrophil inflammation (blue arrow), which resulted in the disorganized pulmonary alveoli structure. LTA-SeNPs had no significant effect on these histopathological alterations. However, the aggravation of lung injury was observed in the Na$_2$SeO$_3$ treated group.

4. Discussion

Though the previous studies suggested that SeNPs has the potential in treating diseases such as cancer, diabetes and Alzheimer's disease, the beneficial effects were only based on short-term experiments with no longer than 13-week treatment to the best of our knowledge [11–13]. Our previous study showed that oral administration of SeNPs for 8 or 12 weeks significantly alleviated hyperlipidaemia and vascular injury in ApoE$^{-/-}$ mice, implying a potential for the prevention of AS [22,23]. However, in this work, 24-week administration of SeNPs showed no benefit and even exacerbated the formation of AS in ApoE$^{-/-}$ mice (Fig. 2), indicative of cardiovascular toxicity. This work is the first time to evaluate the long-term effects of SeNPs, which reveals a potential cardiovascular toxicity of SeNPs after long-term administration. The opposite effects of SeNPs after short-term and long-term administration further confirm the necessity for exploring long-term effects of nanomaterials, particularly those with promising biomedical applications *in vivo*.

The mechanisms by which long-term administration of SeNPs exacerbated atherosclerotic lesions might involve two aspects. First, oxidative stress, which is likely resulted from the imbalance of oxidants and antioxidants occurred in cells, is a critical risk factor of AS [35,36]. In the present study, we found that LTA-SeNPs had no effect on lipid peroxidation, but significantly decreased the activity of serum SOD and GPx in ApoE$^{-/-}$ mice (Table 1). SOD, a key antioxidant enzyme, catalyzes the dismutation of superoxide into H$_2$O$_2$ and oxygen [37]. GPx, the most abundant selenoproteins in mammals, reduce lipid hydroperoxides to their corresponding alcohols and H$_2$O$_2$ to water [10]. The decreased activities of SOD and GPx in the organism are consistent with increased oxidative stress. In addition, the biological effects of Se in the body are largely mediated by selenoproteins or selenoenzymes, in which Se is incorporated as selenocysteine (Sec), the 21st naturally occurring amino acid in the genetic code. The best-known selenoenzymes are GPx and TrxR, which play key roles in antioxidant defense and the regulation of cellular redox signalling [10]. The expressions of three antioxidant selenoenzymes, GPx1, TrxR1 and TrxR2, were inhibited significantly in the liver of LTA-SeNPs treated mice (Fig. 3). GPx1 deficiency led to increased oxidative stress and accelerated atherosclerotic lesion progression in ApoE$^{-/-}$ mice [38,39]. TrxR, ubiquitous thiol oxidoreductases, play positive roles in alleviating AS and related cardiovascular diseases by limiting oxidative stress [40]. Therefore, our results suggested that LTA-SeNPs might induce oxidative stress by inhibiting the activities of antioxidant enzymes and the expression of antioxidant selenoenzymes, which might partially contribute to the aggravated atherosclerotic lesion in HFD fed ApoE$^{-/-}$ mice.

Secondly, hyperlipidaemia has been demonstrated as another risk factor related to atherosclerotic acceleration [41]. Hyperlipidaemia is defined as the abnormal increase of TG, TC and LDL-C (bad cholesterol)

or the abnormal reduced of HDL-C (good cholesterol) in serum [41,42]. It has been reported that SeNPs treatment for 28 days significantly decreased serum lipids level in diabetic rats [19]. Our previous study found that administration of SeNPs for 8 or 12 weeks ameliorated hyperlipidaemia efficiently in ApoE$^{-/-}$ mice [22,23]. However, in the present study, our data showed that the levels of serum TG, TC and LDL-C were further increased in LTA-SeNPs treated mice (Table 2). In the meanwhile, the extremely high level of serum HDL-C (even higher than that in the WT group) was observed in the LTA-SeNPs treated mice. HDL-C is usually considered as a good cholesterol which can prevent AS, however, recent studies have reported the extremely high level of HDL-C is potentially deleterious to cardiovascular system since elevated HDL-C is associated to systemic inflammation and endothelial dysfunction [43,44]. Our results exhibited an enhancing effect of LTA-SeNPs on hyperlipidaemia, which might provide another explanation for the aggravated atherosclerotic lesion. The enhancing effect of LTA-SeNPs on hyperlipidaemia might be partly due to their regulation on the metabolism of cholesterol and fatty acid in liver. Our results showed that LTA-SeNPs induced hepatic lipid metabolic disorder, as demonstrated by the decreased expressions of LDLR, CYP7A1 and ABCG5, three key enzymes involved in cholesterol metabolism, and the increased expression of FAS, a key enzyme involved in fatty acid biosynthesis (Fig. 5). These abnormal effects of LTA-SeNPs on hepatic lipid metabolism further resulted in accumulation of lipid in the liver (Fig. 4).

The biosafety of the nanomaterials is an essential concern when it comes to design of nanomedicine for biomedical applications [5]. Previous animal studies have reported that the short-term toxicity, subchronic and acute toxicity of SeNPs in mice or rats were less than those of traditional Se species such as selenious acid, sodium selenite, SeMet and SeMSC [14–16]. In order to further confirm the long-term toxicity of SeNPs, a series of experiments, including examination of the body weight, serum biochemistry indices and the histopathology of main organs, were performed in HFD fed ApoE$^{-/-}$ mice in this work. LTA-SeNPs had no significant effect on body weight, but showed obvious damage to liver and kidney, as evidenced by the increasing ALT activity and BUN as well as the extensive histopathological changes (Table 3 and Fig. 6). These results suggested that SeNPs after long-term administration had liver and kidney toxicity to animals. However, as a comparison, our data demonstrated that the long-term toxicity of SeNPs was still lower than that of Na$_2$SeO$_3$.

With a given geometric shape, the size of a nanomaterial is a strong determinant of cell uptake and biological actions [45]. Among the tested SeNPs, the long-term toxicity of SeNPs-1 (23.1 nm) and SeNPs-2 (40.4 nm) was higher than that of SeNPs-3 (86.8 nm), and SeNPs-2 showed the highest toxicity. The highest toxicity of SeNPs-2 might be due to its effective cellular uptake. It has been reported that the uptake of mesoporous silica nanoparticles (ranging from 30 to 280 nm) by HeLa cells was size-dependent, with maximum uptake at the size of 50 nm [46]. Moreover, although all gold and silver nanoparticles within the 2–100 nm size range altered signalling processes essential for basic cell functions (including cell death), 40- and 50-nm nanoparticles demonstrated the greatest effect [24]. In the present study, an optimal cellular uptake of SeNPs might be achieved in the SeNPs-2 (40.4 nm) treated ApoE$^{-/-}$ mice and resulted in the worst adverse effects. In addition to the physical properties such as size, shape, and surface charge, the biological actions of nanoparticles are more dependent on chemical composition. For example, for spherical gold nanoparticles and single-walled carbon nanotubes, although a 50-nm diameter is optimal for cellular uptake and accumulation, single-walled carbon nanotubes and gold nanoparticles, each 50 nm in diameter, possess endocytosis rates of 10^{-3} min^{-1} and 10^{-6} min^{-1}, respectively. This 1000-fold difference may be due to the distinct intrinsic properties of carbon versus gold [47]. In this work, although long-term administration of SeNPs-2 (40.4 nm) showed the highest adverse effects, no significant difference was observed among the SeNPs with different sizes. This means that the long-term toxicity of SeNPs was largely dependent on its chemical intrinsic properties.
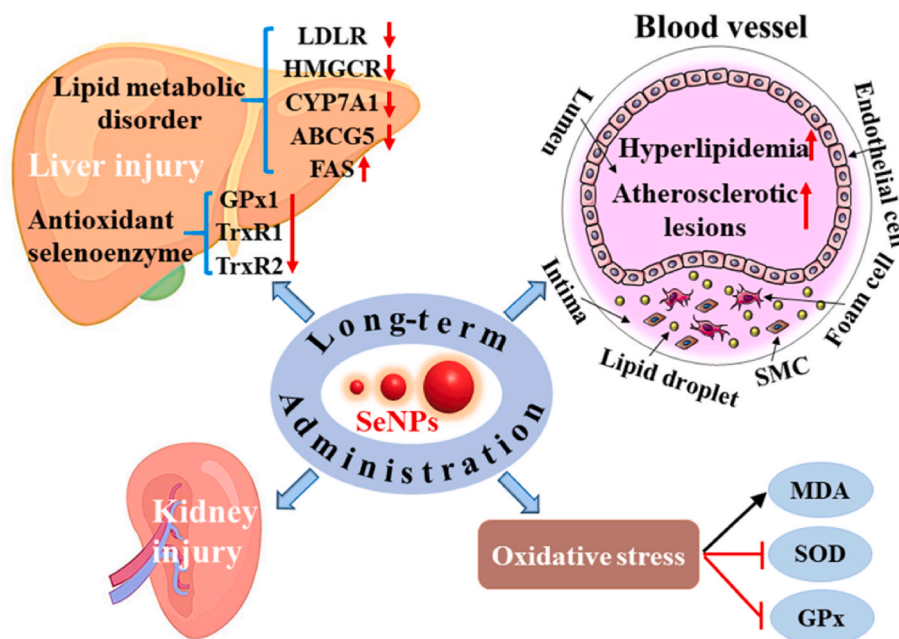
Fig. 7. Schematic diagram for the aggravated effects of long-term administration of SeNPs with different sizes on atherosclerotic lesions and organ injury in ApoE$^{-/-}$ mice induced by a high-fat diet and the proposed mechanism.

BSA was widely used to modify the surface of nanomaterials due to its non-toxic, good biocompatibility, hydrophilicity and biodegradability [48]. In our previous work [25] and this work, BSA was used as a stabilizer or capping agent to control SeNPs size and maintain SeNPs stabilization in aqueous solution. Our previous work demonstrated that the amount of BSA in as-synthesized SeNPs was very low (only 0.68%) [25]. It is well-known that introducing a xenobiotic agent may elicit immune response, oxidative stress, and inflammatory effects etc. Whether such low level of BSA present in SeNPs will elicit these responses remains unknown. Very recently, Park et al. reported that cloaking silica nanoparticles with BSA coating can inhibit nanoparticle-induced complement activation and macrophage uptake, two of the most clinically relevant innate immune reactions related to nanomedicines [49]. Therefore, the exact role (immune response activator or inhibitor) of BSA present in SeNPs should be deeply investigated in the future study.

The present study also raises questions to be answered. Firstly, how are SeNPs metabolized in and/or removed from the body? Especially, the detailed mechanism of uptake of the orally administered SeNPs in the gastrointestinal tract (GIT) and the way of SeNPs entering circulation remain unclear. It is very important to study the fate of SeNPs in the body for fully understanding the toxicological properties of SeNPs. Secondly, in addition to size, the surface charge of the nanomaterials also affects cell uptake and consequently the toxicity. Further studies aimed at addressing the relationship between the surface charge of SeNPs and its long-term toxicity are needed.

5. Conclusions

In this work, we found that LTA-SeNPs even at a low dose aggravated atherosclerotic lesions in HFD fed ApoE$^{-/-}$ mice. The underlying mechanisms may involve (1) exacerbated oxidative stress caused by reduced activities of antioxidant enzymes (SOD and GPx1) and expression levels of antioxidant selenoenzymes (GPx1, TrxR1 and TrxR2), and (2) exacerbated hyperlipidaemia caused by hepatic lipid metabolic disorder. In addition, LTA-SeNPs led to aggravated liver and kidney injury induced by HFD in ApoE$^{-/-}$ mice (Fig. 7). The extent of these adverse effects of SeNPs was size dependent with SeNPs of 40.4 nm in diameter showing the most serious adverse effect among the tested SeNPs ranging from 23.1 to 86.8 nm. These findings provide novel insights for better understanding the biosafety of SeNPs, and may shed light on the research of other biomedical nanomaterials.

CRediT authorship contribution statement

Junying Xiao: Investigation, Conceptualization, Methodology, Project administration, Writing – original draft. **Hui Cao:** Investigation, Methodology, Data curation, Formal analysis. **Siyu Guo:** Investigation, Methodology, Data curation, Formal analysis. **Shengze Xiao:** Investigation, Methodology, Data curation, Formal analysis. **Na Li:** Investigation, Methodology, Data curation, Formal analysis. **Min Li:** Investigation, Methodology, Data curation, Formal analysis. **Yuzhou Wu:** Writing – review & editing. **Hongmei Liu:** Conceptualization, Resources, Writing – review & editing, Supervision, Funding acquisition.

Declaration of competing interest

The authors declare that they have no known competing financial interests or personal relationships that could have appeared to influence the work reported in this paper.

DLS and XRD and also thank the Research Core Facilities for Life Science (HUST) for help in the operation of TEM.

Appendix A. Supplementary data

Supplementary data to this article can be found online at https://doi.org/10.1016/j.cbi.2021.109601.

Author statement

We confirm that all authors listed have contributed to the work, and have read, approved and agreed to submit the manuscript to Chemico-Biological Interactions. The manuscript is new and original and not under consideration for publication elsewhere. There are no conflicts to declare in this work.

References

[1] K.P. Loh, D. Ho, G.N.C. Chiu, D.T. Leong, G. Pastorin, E.K. Chow, Clinical applications of carbon nanomaterials in diagnostics and therapy, Adv. Mater. 30 (2018) e1802368, https://doi.org/10.1002/adma.201802368.

[2] C. Murugan, V. Sharma, R.K. Murugan, G. Malaimegu, A. Sundaramurthy, Two-dimensional cancer theranostic nanomaterials: synthesis, surface functionalization and applications in phototherapy, J. Contr. Release 299 (2019) 1–20, https://doi.org/10.1016/j.jconrel.2019.02.015.

[3] Y. Chen, H. Chen, J. Shi, In vivo bio-safety evaluations and diagnostic/therapeutic applications of chemically designed mesoporous silica nanoparticles, Adv. Mater. 25 (2013) 3144–3176, https://doi.org/10.1002/adma.201205292.

[4] S.A. Love, M.A. Maurer-Jones, J.W. Thompson, Y.S. Lin, C.L. Haynes, Assessing nanoparticle toxicity, Annu. Rev. Anal. Chem. 5 (2012) 181–205, https://doi.org/10.1146/annurev-anchem-062011-143134.

[5] S. Zhu, L. Li, Z. Gu, C. Chen, Y. Zhao, 15 years of small: research trends in nanosafety, Small 16 (2020) e2000980, https://doi.org/10.1002/smll.202000980.

[6] N. Chen, H. Wang, Q. Huang, J. Li, J. Yan, D. He, C. Fan, H. Song, Long-term effects of nanoparticles on nutrition and metabolism, Small 10 (2014) 3603–3611, https://doi.org/10.1002/smll.201303635.

[7] W. Najahi-Missaoui, R.D. Arnold, B.S. Cummings, Safe nanoparticles: are we there yet? Int. J. Mol. Sci. 22 (2020) 385–406, https://doi.org/10.3390/ijms22010385.

[8] S. Barbara, K. Natalia, S. Ewa, G. Marta, J. Slawomir, K. Marta, W. Mateusz, H. Anna, L. Ludwika, C. André, Long term influence of carbon nanoparticles on health and liver status in rats, PloS One 10 (2015) e0144821, https://doi.org/10.1371/journal.pone.0144821.

[9] M.P. Rayman, Selenium and human health, Lancet 379 (2012) 1256–1268, https://doi.org/10.1016/s0140-6736(11)61452-9.

[10] V.M. Labunskyy, D.L. Hatfield, V.N. Gladyshev, Selenoproteins: molecular pathways and physiological roles, Physiol. Rev. 94 (2014) 739–777, https://doi.org/10.1152/physrev.00039.2013.

[11] F. Maiyo, M. Singh, Selenium nanoparticles: potential in cancer gene and drug delivery, Nanomedicine 12 (2017) 1075–1089, https://doi.org/10.2217/nnm-2017-0024.

[12] D. Constantinescu-Aruxandei, R.M. Frincu, L. Capra, F. Oancea, Selenium analysis and speciation in dietary supplements based on next-generation selenium ingredients, Nutrients 10 (2018) 1466–1499, https://doi.org/10.3390/nu10101466.

[13] T.M. Sakr, M. Korany, K.V. Katti, Selenium nanomaterials in biomedicine-An overview of new opportunities in nanomedicine of selenium, J. Drug Deliv. Sci. Technol. 46 (2018) 223–233, https://doi.org/10.1016/j.jddst.2018.05.023.

[14] J. Zhang, H. Wang, X. Yan, L. Zhang, Comparison of short-term toxicity between Nano-Se and selenite in mice, Life Sci. 76 (2005) 1099–1109, https://doi.org/10.1016/j.lfs.2004.08.015.

[15] J. Zhang, X. Wang, T. Xu, Elemental selenium at nano size (Nano-Se) as a potential chemopreventive agent with reduced risk of selenium toxicity: comparison with se-methylselenocysteine in mice, Toxicol. Sci. 101 (2008) 22–31, https://doi.org/10.1093/toxsci/kfm221.

[16] H. Wang, J. Zhang, H. Yu, Elemental selenium at nano size possesses lower toxicity without compromising the fundamental effect on selenoenzymes: comparison with selenomethionine in mice, Free, Radical. Res. 42 (2007) 1524–1533, https://doi.org/10.1016/j.freeradbiomed.2007.02.013.

[17] X. Jia, N. Li, J. Chen, A subchronic toxicity study of elemental Nano-Se in Sprague-Dawley rats, Life Sci. 76 (2005) 1989–2003, https://doi.org/10.1016/j.lfs.2004.09.026.

[18] G. Zhao, X. Wu, P. Chen, L. Zhang, C.S. Yang, J. Zhang, Selenium nanoparticles are more efficient than sodium selenite in producing reactive oxygen species and hyper-accumulation of selenium nanoparticles in cancer cells generates potent therapeutic effects, Free Radical Biol. Med. 126 (2018) 55–66, https://doi.org/10.1016/j.freeradbiomed.2018.07.017.

[19] S. Al-Quraishy, M.A. Dkhil, A.E. Abdel Moneim, Anti-hyperglycemic activity of selenium nanoparticles in streptozotocin-induced diabetic rats, Int. J. Nanomed. 10 (2015) 6741–6756, https://doi.org/10.2147/IJN.S91377.

[20] C.K. Glass, J.L. Witztum, Atherosclerosis: the road ahead,, Cell 104 (2001) 503–516, https://doi.org/10.1016/S0092-8674(01)00238-0.

[21] A. Timmis, N. Townsend, C.P. Gale, A. Torbica, M. Lettino, S.E. Petersen, E. A. Mossialos, A.P. Maggioni, D. Kazakiewicz, H.T. May, D. De Smedt, M. Flather, L. Zuhlke, J.F. Beltrame, R. Huculeci, L. Tavazzi, G. Hindricks, J. Bax, B. Casadei, S. Achenbach, L. Wright, P. Vardas, European Society of Cardiology, European society of cardiology: cardiovascular disease statistics 2019 (executive summary), Eur. Heart J. 6 (2020) 7–9, https://doi.org/10.1093/ehjqcco/qcz065.

[22] S. Xiao, L. Mao, J. Xiao, Y. Wu, H. Liu, Selenium nanoparticles inhibit the formation of atherosclerosis in apolipoprotein E deficient mice by alleviating hyperlipidemia and oxidative stress, Eur, J. Pharmacol. 902 (2021), 174120, https://doi.org/10.1016/j.ejphar.2021.174120.

[23] L. Guo, J. Xiao, H. Liu, H. Liu, Selenium nanoparticles alleviate hyperlipidemia and vascular injury in ApoE-deficient mice by regulating cholesterol metabolism and reducing oxidative stress, Metall 12 (2020) 204–217, https://doi.org/10.1039/c9mt00215d.

[24] W. Jiang, B.Y. Kim, J.T. Rutka, W.C. Chan, Nanoparticle-mediated cellular response is size-dependent, Nat. Nanotechnol. 3 (2008) 145–150, https://doi.org/10.1038/nnano.2008.30.

[25] H. Cao, J. Xiao, H. Liu, Enhanced oxidase-like activity of selenium nanoparticles stabilized by chitosan and application in a facile colorimetric assay for mercury (II), Biochem. Eng. J. 152 (2019), 107384, https://doi.org/10.1016/j.bej.2019.107384.

[26] A.S. Plump, J.D. Smith, T. Hayek, K. Aalto-Setl, A. Walsh, J.G. Verstuyft, E. M. Rubin, J.L. Breslow, Severe hypercholesterolemia and atherosclerosis in apolipoprotein E-deficient mice created by homologous recombination in ES cells, Cell 71 (1992) 343–353, https://doi.org/10.1016/0092-8674(92)90362-G.

[27] Q. Zhang, J. Hu, Y. Wu, H. Luo, W. Meng, B. Xiao, X. Xiao, Z. Zhou, F. Liu, Rheb (ras homolog enriched in brain 1) deficiency in mature macrophages prevents atherosclerosis by repressing macrophage proliferation, inflammation, and lipid uptake, Arterioscler. Thromb. Vasc. Biol. 39 (2019) 1787–1801, https://doi.org/10.1161/ATVBAHA.119.312870.

[28] S. Yang, W. Zhang, L.L. Xuan, F.F. Han, Y.L. Lv, Z.R. Wan, H. Liu, L.L. Ren, L. L. Gong, L.H. Liu, Akebia Saponin D inhibits the formation of atherosclerosis in ApoE(-/-) mice by attenuating oxidative stress-induced apoptosis in endothelial cells, Atherosclerosis 285 (2019) 23–30, https://doi.org/10.1016/j.atherosclerosis.2019.04.202.

[29] K.J. Livak, T.D. Schmittgen, Analysis of relative gene expression data using real-time quantitative PCR and the 2(-Delta Delta C(T)) Method, Methods 25 (2001) 402–408, https://doi.org/10.1006/meth.2001.1262.

[30] G.V.D. Berghe, The role of the liver in metabolic homeostasis: implications for inborn errors of metabolism,, J. Inherit. Metab. Dis. 14 (1991) 407–420, https://doi.org/10.1007/BF01797914.

[31] C. Vantaggiato, E. Panzeri, A. Citterio, G. Orso, M. Pozzi, Antipsychotics promote metabolic disorders disrupting cellular lipid metabolism and trafficking, Trends Endocrinol, Metab. 30 (2019) 189–210, https://doi.org/10.1016/j.tem.2019.01.003.

[32] M.S. Brown, J.L. Goldstein, Multivalent feedback regulation of HMG CoA reductase, a control mechanism coordinating isoprenoid synthesis and cell growth, J. Lipid Res. 21 (1980) 505–517, https://doi.org/10.1016/S0022-2275(20)42221-7.

[33] C.R. Pullinger, C. Eng, G. Salen, S. Shefer, A.K. Batta, S.K. Erickson, A. Verhagen, C. R. Rivera, S.J. Mulvihill, M.J. Malloy, J.P. Kane, Human cholesterol 7α-hydroxylase (CYP7A1) deficiency has a hypercholesterolemic phenotype, J. Clin. Invest. 110 (2002) 109–117, https://doi.org/10.1172/jci200215387.

[34] X.H. Yu, K. Qian, N. Jiang, X.L. Zheng, F.S. Cayabyab, C.K. Tang, ABCG5/ABCG8 in cholesterol excretion and atherosclerosis, Clin. Chim. Acta 428 (2014) 82–88, https://doi.org/10.1016/j.cca.2013.11.010.

[35] D. Harrison, K.K. Griendling, U. Landmesser, B. Hornig, H. Drexler, Role of oxidative stress in atherosclerosis, J. Am. Coll. Cardiol. 91 (2003) 7–11, https://doi.org/10.1016/s0002-9149(02)03144-2.

[36] P.C. Schulze, R.T. Lee, Oxidative stress and atherosclerosis, Curr. Atherosclerosis Rep. 7 (2005) 242–248, https://doi.org/10.1007/s11883-005-0013-5.

[37] I.N. Zelko, T.J. Mariani, R.J. Folz, Superoxide dismutase multigene family: a comparison of the CuZn-SOD (SOD1), Mn-SOD (SOD2), and EC-SOD (SOD3) gene structures, evolution, and expression, Free Radical Biol. Med. 33 (2002) 337–349, https://doi.org/10.1016/S0891-5849(02)00905-X.

[38] M. Torzewski, V. Ochsenhirt, A.L. Kleschyov, A. Daiber, H. Li, H. Rossmann, S. Tsimikas, K. Reifenberg, F. Cheng, H.A. Lehr, S. Blankenberg, U. Forstermann, T. Munzel, K.J. Lackner, Deficiency of glutathione peroxidase-1 accelerates the progression of atherosclerosis in apolipoprotein E-deficient mice, Arterioscler. Thromb. Vasc. Biol. 27 (2007) 850–857, https://doi.org/10.1161/01.ATV.0000258809.47285.07.

[39] P. Lewis, N. Stefanovic, J. Pete, A.C. Calkin, S. Giunti, V. Thallas-Bonke, K. A. Jandeleit-Dahm, T.J. Allen, I. Kola, M.E. Cooper, J.B. de Haan, Lack of the antioxidant enzyme glutathione peroxidase-1 accelerates atherosclerosis in diabetic apolipoprotein E-deficient mice, Circulation 115 (2007) 2178–2187, https://doi.org/10.1161/CIRCULATIONAHA.106.664250.

[40] C.J. World, H. Yamawaki, B.C. Berk, Thioredoxin in the cardiovascular system, J. Mol. Med. 84 (2006) 997–1003, https://doi.org/10.1007/s00109-006-0109-6.

[41] D. Steinberg, Atherogenesis in perspective: hypercholesterolemia and inflammation as partners in crime, Nat. Med. 8 (2002) 1211–1217, https://doi.org/10.1038/nm1102-1211.

[42] U.J. Tietge, Hyperlipidemia and cardiovascular disease: inflammation, dyslipidemia, and atherosclerosis, Curr. Opin. Lipidol. 25 (2014) 94–95, https://doi.org/10.1097/MOL.0000000000000051.

[43] S.T. Chiesa, M. Charakida, E. McLoughlin, H.C. Nguyen, G. Georgiopoulos, L. Motran, Y. Elia, M.L. Marcovecchio, D.B. Dunger, R.N. Dalton, D. Daneman,

E. Sochett, F.H. Mahmud, J.E. Deanfield, Elevated high-density lipoprotein in adolescents with Type 1 diabetes is associated with endothelial dysfunction in the presence of systemic inflammation, Eur. Heart J. 40 (2019) 3559–3566, https://doi.org/10.1093/eurheartj/ehz114.

[44] Y. Takaeko, S. Matsui, M. Kajikawa, T. Maruhashi, S. Kishimoto, H. Hashimoto, Y. Kihara, E. Hida, K. Chayama, C. Goto, Y. Aibara, F.M. Yusoff, K. Noma, A. Nakashima, Y. Higashi, Association of extremely high levels of high-density lipoprotein cholesterol with endothelial dysfunction in men, J. Clin. Lipidol. 13 (2019) 664–672, https://doi.org/10.1016/j.jacl.2019.06.004.

[45] A. Albanese, P.S. Tang, W.C.W. Chan, The effect of nanoparticle size, shape, and surface chemistry on biological systems, Annu. Rev. Biomed, Eng. Times 14 (2012) 1–16, https://doi.org/10.1146/annurev-bioeng-071811-150124.

[46] F. Lu, S.H. Wu, Y. Hung, C.Y. Mou, Size effect on cell uptake in well-suspended, uniform mesoporous silica nanoparticles, Small 5 (2010) 1408–1413, https://doi.org/10.1002/smll.200900005.

[47] H. Jin, D.A. Heller, R. Sharma, M.S. Strano, Size-dependent cellular uptake and expulsion of single-walled carbon nanotubes: single particle tracking and a generic uptake model for nanoparticles, ACS Nano 3 (2009) 149–158, https://doi.org/10.1021/nn800532m.

[48] J. Wang, B. Zhang, Bovine serum albumin as a versatile platform for cancer imaging and therapy, Curr. Med. Chem. 25 (2018) 2938–2953, https://doi.org/10.2174/0929867324666170314143335.

[49] J.H. Park, J.A. Jackman, A.R. Ferhan, J.N. Belling, N.J. Cho, Cloaking silica nanoparticles with functional protein coatings for reduced complement activation and cellular uptake, ACS Nano 14 (2020) 11950–11961, https://doi.org/10.1021/acsnano.0c05097.